# Effect of TiOx Surface Modification on the Electrochemical Performances of Ni-Rich (NMC-622) Cathode Material for Lithium-Ion Batteries

Peer-reviewed author version

MYLAVARAPU, Satish Kumar; ULU, Fulya; YARI, Saeed; DE SLOOVERE, Dries; D'HAEN, Jan; SHAFIQUE, Ahmed; VAN BAEL, Marlies; SAFARI, Momo & HARDY, An (2021) Effect of TiOx Surface Modification on the Electrochemical Performances of Ni-Rich (NMC-622) Cathode Material for Lithium-Ion Batteries. In: Acs Applied Energy Materials, 4 (10), p. 10493-10504.

DOI: 10.1021/acsaem.1c01309
Handle: http://hdl.handle.net/1942/35510

# "Effect of $TiO_x$ surface modification on the electrochemical performances of Ni-rich (NMC-622) cathode material for lithium-ion batteries"

*Satish Kumar MYLAVARAPU [a,b,c], Fulya Ulu Okudur [a,b,c], Saeed Yari [b,c,e], Dries De Sloovere [a,b,c], Jan D'Haen[d], Ahmed Shafique [a,b,c,f] Marlies K. Van Bael [a,b,c], Mohammadhosein Safari [b,c,e] and An Hardy [a,b,c] **

[a] *Hasselt University, Institute for Materials Research (IMO-IMOMEC), Materials Chemistry, DESINe Group, Agoralaan Building D, 3590, Diepenbeek, Belgium*

[b] *EnergyVille 2, Thor park 8320, 3600 Genk, Belgium*

[c] *IMEC division, IMOMEC, Wetenschapspark 1, 3590 Diepenbeek, Belgium*

[d] *Hasselt University, Institute for Materials Research (IMO-IMOMEC), Materials Physics, ELPHYC Group, Wetenschapspark 1, 3590, Diepenbeek, Belgium*

[e] *Hasselt University, Institute for Materials Research (IMO-IMOMEC), Engineering Materials and Applications (EMAP), Electrochemical Engineering Group, Wetenschapspark 1 3590, Diepenbeek, Belgium*

[f] *Sustainable Materials, VITO (Flemish Institute for Technological Research), 2400 Mol, Belgium*

**Abstract:**

Ni-rich layered lithium transition metal oxides ($LiNi_xMn_yCo_zO_2$) have gained significant attention as high capacity positive electrode materials for lithium-ion batteries. However, their poor cyclability, capacity retention and rate capability at higher working potentials limit their applications in commercial batteries. Here, we demonstrate a cost-effective chemical solution deposition route of a thin $TiO_x$ shell on $LiNi_{0.6}Mn_{0.2}Co_{0.2}O_2$ (NMC-622)

particles and the effect of surface modification on the electrochemical properties. The crystallinity and morphology of the NMC-622 particles are unaffected by the deposition step, verified by powder X-ray diffraction and electron microscopy. HRTEM and SAED analysis showed the $TiO_x$ surface layer is amorphous and prone to enhance the electronic conductivity of the cathode material. The $TiO_x$-coated material has an improved rate performance and experiences a lower charge transfer resistance compared to the pristine material. The effect of the surface modification on the electrochemical performance of NMC-622 was investigated further by the assembly of NMC-622/$Li_4Ti_5O_{12}$ (LTO) full cells. The beneficial impact of the $TiO_x$ coating on the electrochemical performance of NMC-622 positive electrodes in lithium-ion battery applications was showcased by the higher initial Coulombic efficiency and lower aging rates during 150 cycles at 1C in NMC-622/LTO cells.

**Keywords:** Lithium-ion batteries, Ni-rich layered NMC, surface modification, amorphous $TiO_x$ coating, and capacity retention

**Introduction:**

Since the commercialization of rechargeable lithium-ion batteries in the 90's, the main research focus has shifted to the development of high energy density batteries for portable electronics, and more recently, for electric mobility in an effort to reduce the consumption of non-renewable resources and $CO_2$ emissions[1,2]. Ni-rich layered lithium transition metal oxides ($LiNi_xMn_yCo_zO_2$; NMC) are among the best alternatives for the original $LiCoO_2$ and belong to the high capacity $LiNiO_2$ material family[3,4,5,6]. When cycled at higher working potentials, Ni-rich NMC positive electrode materials are vulnerable to capacity fade and premature end of life[7]. Such degradation is induced by mechanical instability, parasitic reactions, and low NMC conductivity values[8,9].

A recent report by, Ruan et al.[10] summarizes the capacity degradation mechanisms and structural evolution of Ni-rich NMC at higher working voltages. They summarized that the

upper cut-off voltage limit has a significant influence on capacity decay and on the parasitic reactions at the surface. When charged up to 4.8/4.7 V vs $Li^+/Li$, NMC-622 tends to form an insulating surface layer combined with an irreversible change of the bulk lattice[11]. In general, this structural degradation is associated with oxygen loss and irreversible phase transformation. One of the main reasons for the capacity fade is believed to be the cation mixing[12,13]. When $Li^+$ is extracted, $Ni^{2+}$ will migrate out of the transition metal (TM) layer and occupy the vacant $Li^+$ sites in the lithium layer since they have a similar ionic radius ($Ni^{2+}$: 69 pm; $Li^+$: 76 pm)[14,15].

In an effort to mitigate these issues, previous studies reported surface modification[16,17] or surface doping[18,19] techniques to improve the (electro)chemical stability over prolonged cycling[20,21]. Weigel et al.[22] reported that surface doping with multivalent cations ($Al^{3+}$, $Zr^{4+}$, $Ti^{4+}$, $Mg^{2+}$, $Ta^{5+}$) remarkably improved the structural stability and electrochemical performance of Ni-rich NMC. Zhao et al.[23] observed that surface coating can lead to surface doping during high temperature sintering of $LiCoO_2$.

Deposition techniques like atomic layer deposition (ALD), physical vapor deposition (PVD), and chemical vapor deposition (CVD) are costly tools to coat layers on active materials and prepare core-shell particles. ALD also suffers from limited upscaling potential. Still, many researchers have applied ALD[24] to coat layers on positive electrode materials, including Ni-rich NMC materials[25]. Numerous metal oxides such as $Al_2O_3$[26,27], MgO[28], and $TiO_2$[29,30] have been used as coating materials to enhance the electrochemical performances of electrode materials. Also fluorides ($AlF_3$)[31] and phosphates (AlPO(N))[32] were successfully deposited by ALD and improved the electrochemical performance of a number of positive electrode materials. However, several of them show poor ionic and electronic conductivities, thereby compromising the electrode's rate capability[33].

As a flexible and cost-effective alternative, continuous and uniform coatings of metal oxides can also be achieved by wet chemical solution deposition (CSD) routes, allowing to

adapt the surface of core particles[34,35,36,37,38]. The deposition thickness is typically in the order of ten to a few hundred nm thickness[39]. The simple experimental setup and high processing rates constitute considerable advantages to upscale the solution-based synthesis. Hyejung et al.[34] mitigated NMC-622 surface degradation by CSD coating nano-scale $LiCoO_2$ layers as shell material. Gao et al.[40] used CSD to apply a $TiO_2$ coating on NMC-622. The coating procedure also induced some extent of surface $Ti^{4+}$ doping. The combined effect of surface coating and doping suppressed the occurrence of parasitic reactions on the NMC/electrolyte interface. Recently, Fengxia Xin et al[41,42] reported Li-Nb-O coating or ($Nb^{5+}$) substitution via the wet chemical method and enhanced the electrochemical properties of layered Ni-rich cathode material.

Ulu Okudur et al.[43] from our research group reported an amorphous $TiO_x$ surface coating/doping of LNMO *via* a hydrolysis-condensation route, and studied the effect of annealing temperature on the surface and bulk doping of Ti into the LNMO-spinel structure. $TiO_x$ coated LNMO showed superior cycling stability, Coulombic efficiency and rate performances compared to bare LNMO.

$TiO_2$ was selected as the coating material because it is a stable negative electrode material for the lithium-ion batteries in itself[44,45], and as such could possibly store lithium-ions and provides sufficient lithium-ion conductivity at higher current rates and enable to reach higher power densities. The $TiO_2$ coating or Ti-surface doping could enhance the Li-ion diffusion co-efficient and the rate performance. Besides that, $TiO_2$ has a stable structure, which could improve the cathode material's structural stability.

In this work, we assess whether this coating procedure can be extended to other positive electrode materials for lithium-ion batteries: we report the preparation of $TiO_x$ surface coated NMC-622 via a chemical solution deposition route, using ammonia as catalyst in a non-aqueous medium. Furthermore, we study the effect of surface modification on the electrochemical

performance of NMC-622 positive electrodes combined with Li and LTO negative electrodes. The $TiO_x$ surface coating process was performed in an inert atmosphere and in anhydrous ethanol to avoid homogeneous nucleation of $TiO_2$ particles. We show that $TiO_x$ coated NMC-622 has an increased power and energy density compared to NMC used in this study. We ascribe these positive effects to the mitigation of side reactions occurring at the NMC-622/electrolyte interface, which prevents transition metal ion dissolution. The $TiO_x$ coating delivers functional lithium-ion conduction networks. Full cell studies further revealed the improved cyclability and capacity retention of NMC-LTO.

**Experimental:**

***Materials.*** All chemicals in this work are high purity and used without any further purification. $LiNi_{0.6}Mn_{0.2}Co_{0.2}O_2$ (NMC-622, a commercial product) was used as received as core particles. Titanium (IV) butoxide (TBOT, Ti $(OCH_2CH_2CH_2CH_3)_4$, 97%, Sigma Aldrich) was used as Ti source, with absolute ethanol (Merck EMSURE anhydrous, 99.9%, for analysis) as the solvent in the synthesis. Aqueous ammonia (25%, Merck) was used as catalyst and reagent for the hydrolysis of TBOT.

***Synthesis of $TiO_2$@NMC core-shell particles.*** The core-shell particles were prepared by a hydrolysis deposition method catalyzed by ammonia. In a typical experiment, 3 g NMC-622 dispersed in 100ml of absolute anhydrous ethanol (to avoid the presence of moisture before the addition of ammonia, to avoid irreproducibility and side reactions) and sonicated for 15 minutes (Branson bath sonicator, 3510). Aqueous ammonia (0.5 ml) solution was added very quickly (avoiding ammonia evaporation) to the dispersion using a micropipette and the whole was connected to a reflux setup (45˚C, 500 rpm stirring). The titanium precursor was prepared separately by quickly mixing 2.4 ml of TBOT into 17.6 ml absolute anhydrous ethanol in ambient air, just before the addition, avoiding take-up of moisture from the atmosphere. This solution was added dropwise to the NMC-622/ammonia/ethanol dispersion using an auto-

titrator (Schott Geräte, T100, T20) at a flow rate of 1.43 ml/h. The reaction setup was flushed with $N_2$ gas (Air Liquid, Alphagaz 1) with continuous $N_2$ flow to avoid any moisture contact during the addition of TBOT solution. Finally, the reaction mixture was stirred for 6h. At the end of the reaction, the dispersed particles were collected by centrifuging (Eppendorf 5804R, 50ml tubes, 12000 rcf, 10 minutes) four times with intermediate washing with ethanol. The particles were dried (at 80˚C, overnight) and further heat-treated in a tube furnace (500˚C, 3h, 5˚C/min heating rate, 0.5 L/h dry air (Air Liquid, Alphagaz 1)). NMC-622 was similarly treated without titanium precursor and annealed (500°C, 3h, 5°C/min) for better comparison and to see the effect of the wet chemical coating technique.

***Physical characterization.*** The crystalline properties of as prepared core-shell particles were characterized by powder X-ray diffraction analysis (XRD, Bruker AXSD8 Discover diffractometer, Cu K-Alpha radiation, Ni filter, Lynx Eye detector). The particle size distribution and surface morphologies were analyzed using scanning electron microscopy (FEG-SEM, FEI Quanta 200F: only secondary electron images made with ETD (Everhart-Thornley detector) are presented)), EDX spectra were recorded using FEI quanta energy-dispersive X-ray spectroscopy (EDX) detector, and transmission electron microscopy (TEM, FEI Tecnai G2 Spirit Twin, 120 kV). High resolution transmission electron microscopy (HR-TEM), EDX and selected area electron diffraction (SAED) analysis were performed using a FEI Tecnai microscope operated at 200 kV. TEM samples were prepared by dispersing the powder in absolute anhydrous ethanol, sonicating for 1 min, drop-casting onto copper grids coated with a formvar foil (EMS, FCF-200-Cu), and drying under an infrared lamp for a few minutes.

***Electrochemical characterization.*** NMC and surface treated NMC electrodes were prepared by mixing 91 wt.% active material, 4 wt.% carbon black (C-NERGY super C-45) and 5 wt.% polyvinylidene di-fluoride (PVDF, Solvay) dissolved in NMP (Carl Roth chemicals,

99.8%) in a planetary vacuum mixer (Thinky ARV 310 LED) at 2000rpm for 10min under vacuum. The resulting slurry was casted (200 µm wet coating thickness) on a degreased aluminum current collector with 16 µm thickness using a blade coater (MTI). The coatings were subsequently dried at 110˚C for 2h and calendared (reducing the thickness from 50µm to 40µm) to achieve the desired thickness (after calendaring ~40µm) and electrode porosities. Tap density of NMC 622: ~3.1 g/cm$^3$, cathode mass loading 9.3±0.1 mg/cm$^2$, thickness excluding the current collector 40 ±1 µm, porosity 36.6 ±1.6%, electrode density 2.6 ± 0.06 g/cm$^3$).

The electronic conductivity of electrode coatings of both NMC and $TiO_x$ coated NMC-622 was measured using a four-point probe (Ossila, at room temperature). The coatings were prepared on a non-conductive, thermally stable and chemically resistant substrate (Polyimide based Kapton film, DuPont) instead of the current collector. The probes were in-line and equally spaced. The sheet resistance was measured in three locations with 25 iterations at each location.

The following equation was used to calculate the electronic conductivity of the samples at the electrode level,

$$\sigma = \frac{1}{t.R} \qquad \text{(equ.1)}$$

where $\sigma$ (S/cm) is the electronic conductivity, $t$ (µm) is the electrode thickness, and (R, Ohms-cm) is the sheet resistance.

The powder sample's electronic conductivity (the powder resistivity and converted) was measured using a homebuilt setup at a partner research institute VITO at room temperature (details attached in the supporting information). In a typical experiment, the powder samples were placed in the sample holder and applied 1 bar pressure, and the pressure was kept constant for all the samples. Also, we used the same volume (amount) of the sample in all measurements. The electronic conductivity measurements were repeated three times to ensure the reliability of

the data, and the results were averaged. The following equation was used to calculate the electronic conductivity of the powders.

$$\rho = \frac{RA}{l} \quad \text{(equ. 2) \&}$$

$$\sigma = \frac{1}{\rho} \quad \text{(equ. 3)}$$

Where, R is the resistance (Ω), A is the area ($cm^2$), l is the thickness of the sample (μm), ρ is the resistivity (Ω*cm) and σ is the electronic conductivity (S/cm).

NMC-622 half cells (Li metal as the negative electrode) and full cells ($Li_4Ti_5O_{12}$ as the negative electrode) were assembled to study the electrochemical performance. The commercially available LTO electrodes (custom cells GMBH) were used (formulation; AM+ CB+ Binder: 84:8:8, active material loading 12.7 ±0.1 $mg/cm^2$, thickness excluding the current collector 70 ±1 μm, porosity 30 ±0.3%, electrode density 2.14 ± 0.02 $g/cm^3$) in the full cell study. Punches (15 mm diameter) were cut out of the calendared electrodes and dried at 110˚C overnight in a vacuum oven (Büchi), to remove any residual moisture before cell assembly. The samples were then transferred into an argon-filled glove box ($O_2$ and $H_2O$ < 1ppm) to fabricate CR-2025 type coin cells. The separator was a Celgard 2325 polypropylene sheet. As electrolyte, 1M $LiPF_6$ in EC: EMC (3:7 w/v of ethylene carbonate and ethylene methylene carbonate, Soulbrain) with 2 wt.% of VC (vinylene carbonate) was used.

Electrochemical characterization was carried out using a BCS-805 (Bio-Logic) battery tester at room temperature. All coin cells underwent a 24 h open-circuit potential period before beginning galvanostatic cycling. The electrodes were activated by three galvanostatic charge/discharge cycles (formation cycles) at C/10 (1C defined based on 180 mAh as theoretical capacity) between 3.0 V to 4.4 V vs $Li^+/Li$. A rate capability test was performed by (dis)charge cycles at rates ranging from 0.2C to 5C. The electrochemical impedance spectroscopy (EIS, 10 kHz- 100 mHz, 10 mV amplitude) was performed before and after rate

capability tests. The NMC-622/LTO full cells underwent three formation cycles at C/10 (1.4-2.7 V vs $Li^+$/Li, 1C=175 mAh/g). Subsequently, they were galvanostatically cycled between 1.4 V and 2.8 V for long-term constant current (CC) cycling at 1C.

***Results and Discussion:***

**Reaction mechanism:**

***a. Effect of aqueous ammonia on the formation of $TiO_2$ surface layers:***

Kessler et al.,[46,47] reported that in sol-gel synthesis, transition metal alkoxides under hydrolytic or non-hydrolytic conditions tend to form metal oxide nanoparticles through the formation of oxometallate clusters: upon hydrolysis, primary particles form almost instantly. These have an oxide core with ligands on the surface, implying that their size (~5 nm) does not gradually increase. Gelation or precipitation is caused by aggregation of these particles[48].

In general, Ti-alkoxides can follow a homogeneous nucleation pathway in the presence of trace amounts of moisture, leading to the formation of free $TiO_2$ particles[49]. However, the presence of such free $TiO_2$ particles together with active material particles is highly undesirable, as it will lead to a lower capacity of the final cell due to the redundant mass of the non-active $TiO_2$ particles. Therefore, here, the aim is to achieve only heterogeneous nucleation. Li et al.[50] reported a versatile kinetically controlled coating method to coat uniform porous $TiO_2$ shells on various core particles. Here, the effect of the ammonia concentration on the formation of a porous $TiO_2$ shell formation within a mixed solvent was thoroughly investigated, and it was shown that an optimal amount of ammonia will allow to achieve purely heterogeneous nucleation[50]. In the study at hand, the core particles are neither nanoparticles nor unreactive towards ammonia, in the sense that the metal ions can form amine complexes[51]. Therefore, it is worth further investigation for this particular core-shell growth of Titania on NMC surface [52,53].

The TBOT concentration (10 wt.%, or 12 ml) was kept constant and the volume of aq. ammonia was varied to study the effect of ammonia on $TiO_2$ surface coating formation. Figure

1a shows the EDX spectrum of NMC, processed without any aq. ammonia addition. The surface morphologies of NMC and $TiO_x$ coated NMC are shown in the supporting information (SI, figure S1a). Whereas a coating could be observed (figure S1d) for sample processed with 0.5ml of ammonia (10 wt.% of $TiO_x$), this was not the case for sample processed without any ammonia. As shown in the Figure 1b, with a small amount (0.1ml) of ammonia added to the reaction system, no apparent Ti signal from $TiO_x$ could be found in the EDX spectrum. Figure S1b shows the surface morphology of NMC (treated with 0.1ml of ammonia), where no surface layers could be detected. With this low ammonia volume, the deposition rate was very slow, resulting in no significant $TiO_x$ deposition. When the volume of aq. ammonia was increased to 0.3ml, there was a growth of $TiO_x$ nano layers on the surface of NMC particles, which could be hardly observed in the SEM images (shown in Figure S1c), but a very small Ti signal at 4.5 keV was detected in the EDX spectrum, represented in figure 1c. When even higher quantities of aq. ammonia (0.5ml) were used in the reaction system, as depicted in the figure S1d, a uniform $TiO_x$ layer formed on the NMC surface, and the EDX spectra showed a clear indication of the Ti presence at the surface, demonstrated in the figure 1d.

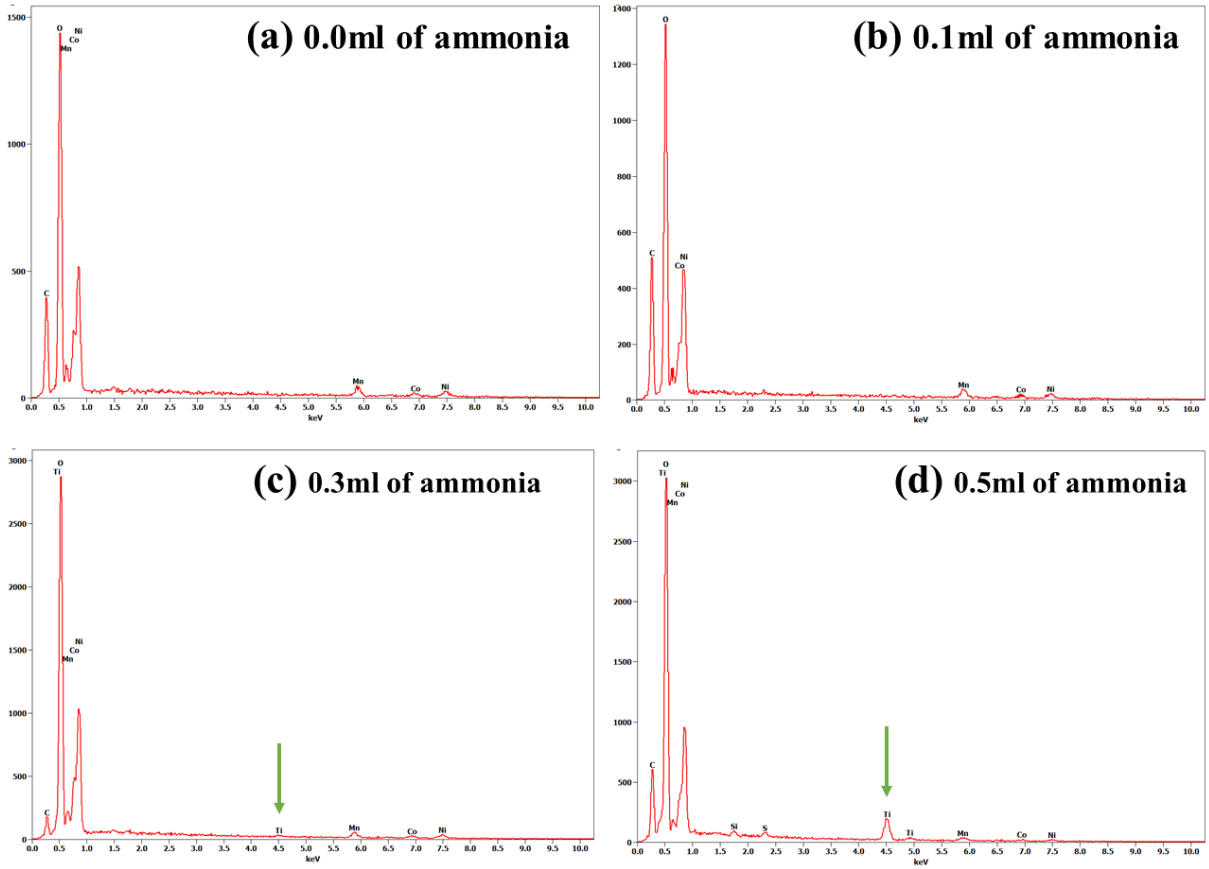


***Figure 1. EDX spectrum of 10 wt.% $TiO_x$ coated NMC, indicating the effect of ammonia concentration on the deposition of $TiO_x$ (a) 0.0ml of ammonia, (b) 0.1ml of ammonia, (c) 0.3ml of ammonia and (d) 0.5ml of ammonia.***

***b. Controlling the thickness of the $TiO_2$ coating layers:***

The $TiO_2$ formation kinetics depend on the quantity of aq. ammonia. It is essential to control the thickness of the $TiO_2$ layers in view of the application. In LIBs, the particle coating/shell layers should be continuous to provide protection but thinner than 15-20 nm to offer sufficient conductivity[54]. Thicker coatings proved to worsen the electrochemical performance of positive electrode materials due to the lithium-ion blocking effect[55]. Low-lithium-ion conducting materials tend to hinder the lithium-ion's intercalation during the fast (dis)charging steps. This means that the kinetics of lithium-ion intercalation and de-intercalation is impeded by the thick non-conducting layers[16]. The coating thickness was controlled by lowering the TBOT concentration, as in agreement with earlier reports [53]. In this case, the TBOT concentration was lowered to 2 wt.% (2.4ml), while keeping aq. ammonia volume (0.5ml) and all other parameters constant in comparison to the previous set of experiments. Figure S2 (supporting information)

shows the surface morphology NMC-622 with two different weight percentages of $TiO_x$: 10 wt.% (Figure S2a) and 2 wt.% (Figure S2b). Thick layer deposition was found in the 10 wt.% $TiO_x$ coated samples. The EDX spectra confirm that by reducing the TBOT concentration, the $TiO_x$ shell thickness was reduced. As shown in figure S2c and S2d, the intensity of the Ti peak (at 4.5 keV) EDX signal in the 10 wt.% $TiO_x$ coated NMC was higher than that of 2 wt.% of $TiO_x$ coated NMC.

***Physical characterizations:***

Based on the above results of $TiO_x$ layers formation on the NMC-622, 2 wt.% $TiO_x$ (and 10 wt.% $TiO_x$) coated samples were further characterized. The powder X-ray diffraction (XRD) patterns of NMC-622 and $TiO_x$ coated NMC-622 are shown in figure 2. Due to the low $TiO_x$ (2 wt.% and 10 wt.% $TiO_x$, logarithmic scale, supporting information; figure S4) content, only the NMC-622 (a layered structure with space group $R\bar{3}m$) diffraction peaks were found, with no evidence of a separate crystalline $TiO_x$ phase within the detection limits of XRD[56,57,58]. Both patterns are in good agreement with the layered structure of NMC-622, where lithium and transition metals (TMs) are arranged in alternate layers, in which lithium atoms occupy octahedral sites ($Li_{Oh}$) in the Li layers and transition metals Ni, Mn and Co ($TM_{Oh}$) occupy the TM layers. It is concluded that the bulk structural properties of the NMC-622 were unaffected by the $TiO_x$ surface coating procedure. Table S1, shows the refined parameters of the NMC and $TiO_x$ coated NMC samples. The results suggest that the some of $Ti^{4+}$ could be surface doped at the NMC structure, as a slight increase in the cell volume and lattice constants been observed. Perhaps this could be related to the larger ionic radii of $Ti^{4+}$ (68 pm) compared to $Co^{3+}$ (54.5 pm) and $Mn^{4+}$ (53 pm).

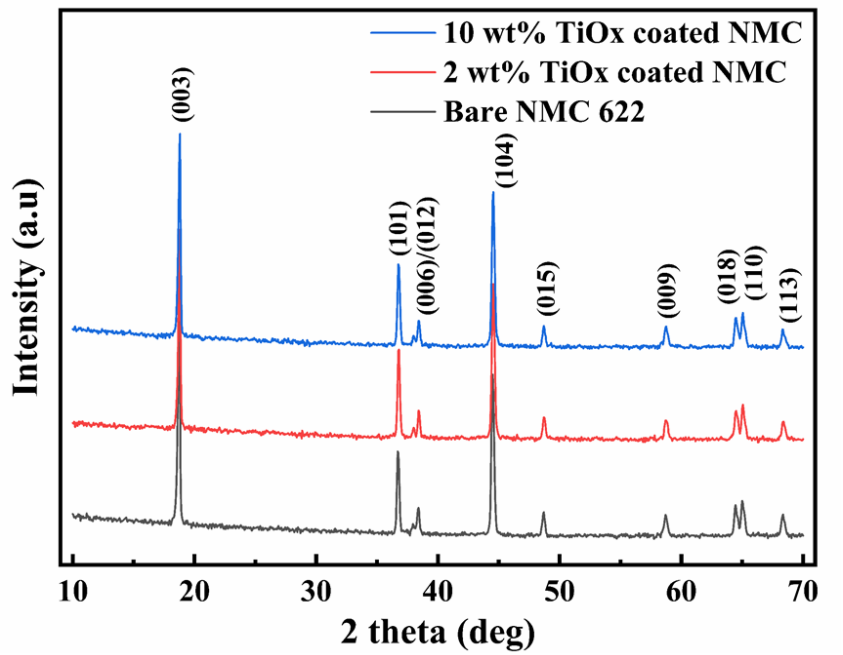


***Figure 2. XRD patterns of NMC, 2 wt.% $TiO_x$ coated NMC and 10 wt.% $TiO_x$ coated NMC after annealing at 500˚C for 3h in DA.***

The morphology of the electrode materials was investigated to visualize the coating process's effect on the morphologies of NMC. Figures 3a and 3b show the SEM-SE (secondary electron/ETD) images of the NMC-622 and 2 wt.% $TiO_x$ coated NMC at lower magnifications. As received NMC-622 secondary particles have an average particle size of 12 µm. These secondary particles are spherical and densely packed with primary particles sizing from 200 to 500 nm, which is beneficial for the volumetric energy density of the electrode materials[59,60].

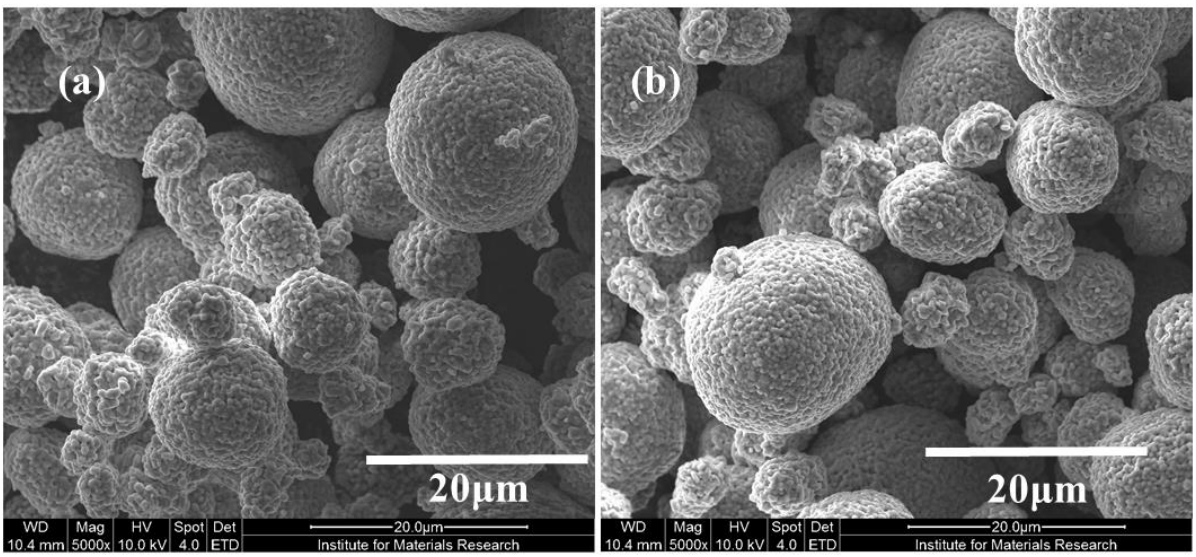


***Figure 3. SEM images of NMC secondary particles (a) and 2 wt. % of $TiO_x$ coated NMC (b).***

Such larger aggregate size of particles is favorable to decrease the surface area in direct contact with the electrolyte and as such decelerate the side reactions at the electrode/electrolyte interface. It can be concluded that the coating process did not change the core morphology at the magnifications that were studied in SEM.

To further investigate the coating efficiency and confirm the presence of $TiO_x$ surface protecting layers, TEM-EDX analysis was performed on the particles. Figures 4a and 4b show the higher magnification TEM images and EDX spectrum of NMC-622, and figures 4c and 4d depict higher magnification images of 2 wt.% $TiO_x$ coated NMC, with an SAED pattern taken at the surface of the $TiO_x$ coating. SAED analysis showed that the layered NMC structure was undisturbed by the $TiO_x$ surface coating/doping. Figure S3 shows the TEM images of 10 wt.% $TiO_x$ coated NMC. Figure S3b depicts the amorphous $TiO_x$ surface layer over the layered NMC structure. From the EDX spectrum of uncoated and coated NMC at the surface layers, a weak signal for Ti was observed at 4.5 keV in the $TiO_x$ coated NMC samples confirming the presence of $TiO_x$ protecting layers at the NMC surface (EDX analysis was performed at different spots at the surface of the NMC). The amount of oxygen in the $TiO_x$ coated NMC is uncertain. During the heat treatment, titanium ions from the $TiO_x$ coating might diffuse into the core particles, resulting in surface doping[43]. It is noteworthy to point out the recent literature which, advises that, regardless of the crystalline or amorphous nature of the $TiO_x$, it acts as an excellent electronically conducting material[61,62]. Besides that the surface modification could perhaps enhance the electronic conductivity/electronic percolation of active (both cathode & anode) materials at the electrode and material level[62]. Furthermore, the electronic conductivity measurements further confirm this on both powder and electrode levels.

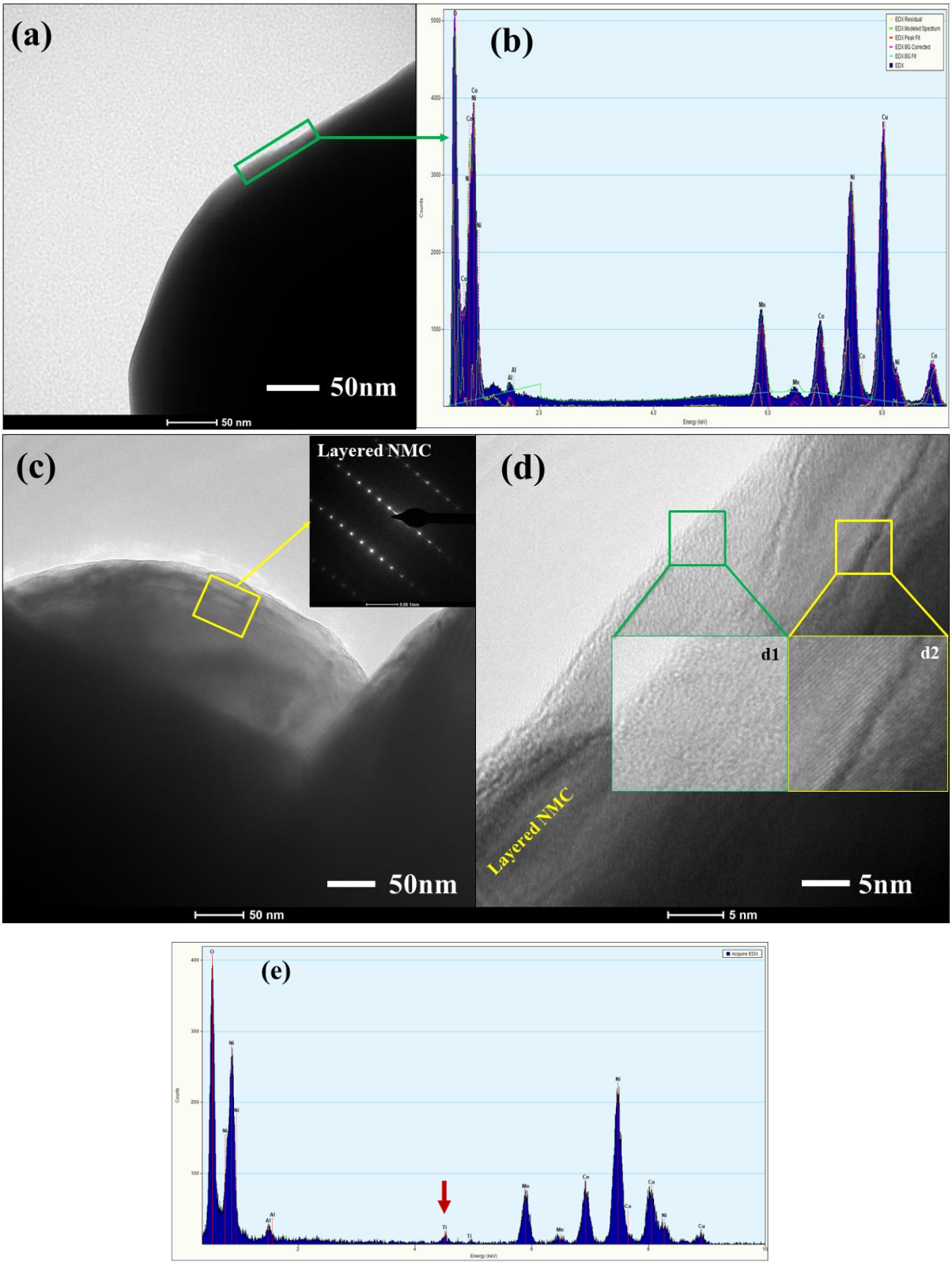


***Figure 4. HR-TEM images of NMC and $TiO_x$ coated NMC. (a) higher magnification image of NMC, (b) EDX spectrum of NMC, (c) 2 wt.% of $TiO_x$ coated NMC (insert is SAED analysis at the surface of the 2 wt.% $TiO_x$ coated NMC), higher resolution of 2 wt.% $TiO_x$ coated NMC (insert at the surface amorphous (d1) and layered NMC pattern (d2)) and (e) EDX of 2 wt.% of $TiO_x$ coated NMC.***

***Electronic conductivity:***

The effect of $TiO_x$ coating on the electronic conductivity of NMC-622 was studied since the electronic conductivity of an electrode material significantly influences the electrochemical performances of a battery, especially at higher charge/discharge rates[63]. Besides the theoretical capacity and loading of the active material, the cathode's energy density also depends on the electronic conductivity of the electrode through improved network connections with the current collector. This is generally ensured by adding conductive additives such as carbon black to the electrode composition, which reduces the net mass of active material in the electrode. Alternatively, the conductivity can be improved without significantly lowering the energy density, by introducing conductive layers on cathode materials while reducing the amount of conductive additives.

The measured thickness of the electrode coating on the non-conductive substrate (Kapton film) is around 70μm for both samples. The conductivity of the NMC electrode was slightly lower than the $TiO_x$ coated NMC electrode. The electronic conductivity vs. number of interactions was plotted for both NMC and $TiO_x$ coated NMC, shown in SI figure S5. There is avg. ca.11% improvement in the electronic conductivity of the $TiO_x$-coated NMC relative to that of the NMC, which is beneficial for the long-range transport of the electrons between the current collector and the NMC particles. Furthermore, to understand the electronic conductivity of the $TiO_x$ surface modification, conductivity measurements were carried out on powder samples and compared. $TiO_x$ surface modified samples showed better electronic conductivity than NMC powders, shown in the supporting information (Table S2). As noticed, 10 wt.% $TiO_x$ coated NMC showed higher electronic conductivity than rest of the samples, which could be related the amorphous $TiO_x$ coating on the NMC particles (figure S3a).

***Electrochemical characterization:***

The effect of the coating procedure on the electrochemical properties of NMC-622 was assessed by incorporation in coin cells. Figure 5a shows the galvanostatic charge-discharge profiles (formation cycles) of NMC and 2 wt.% $TiO_x$ coated NMC-622 in half cell configuration. The 2 wt.% $TiO_x$ coating does not negatively affect the discharge capacity, which remains similar to the capacity of NMC, namely 180 mAh/g at C/10, averaged over three cells. The formation cycles are meant to improve the wetting of the electrode and complete the formation of a thin cathode electrolyte interface (CEI) during the initial lithium (de)intercalation process. The $TiO_x$ coating slightly increased the initial Coulombic efficiency of the electrode, shown in figure 5b. The main reason behind the selection of 2 wt.% of $TiO_x$ coated NMC samples over 10 wt.% $TiO_x$ coated NMC is the thick coating could act as a Li-ion blocking layer and worsen the electrochemical performances of the NMC samples. The electrochemical properties of the 10 wt.% $TiO_x$ coated NMC samples are compared with 2 wt.% $TiO_x$ coated NMC in figure S6 and this indeed supports the argumentation given. Figure S6 shows the comparison of rate capability test of NMC, 2 wt.% $TiO_x$ coated NMC and 10 wt.% $TiO_x$ coated NMC.

Figures 5c and 5d show the rate capability (constant current – constant voltage (CC-CV)) test NMC-622/Li half cells containing either NMC or $TiO_x$ coated positive electrodes. In this mode, the cells were always charged till 4.4V at 0.2C, 0.5C, 1C, 2C, 3C, and 5C, followed by a constant voltage step until the current decreased to C/20. Afterwards, the cells were discharged in the same way until 3V, followed by a CV step (until the current decreased to C/20). The constant-voltage step was used to ensure that the electrodes always reached a similar state of charge before starting the next discharge step. As such, a fair comparison can be made between the delivered discharged capacities at different C-rates[64]. At current rates up to 3C, the effect of the $TiO_x$ on the discharge capacity is negligible (Figure 5c). When the current is further

increased to 5C, the $TiO_x$ coated material showed a significantly higher discharge capacity (ca. 111 mAh/g) than its bare counterpart (ca. 100 mAh/g). Figure 5d shows the capacity retention values normalized to the capacity at 0.2C. At 5C, the coated NMC-622 is able to deliver 74%

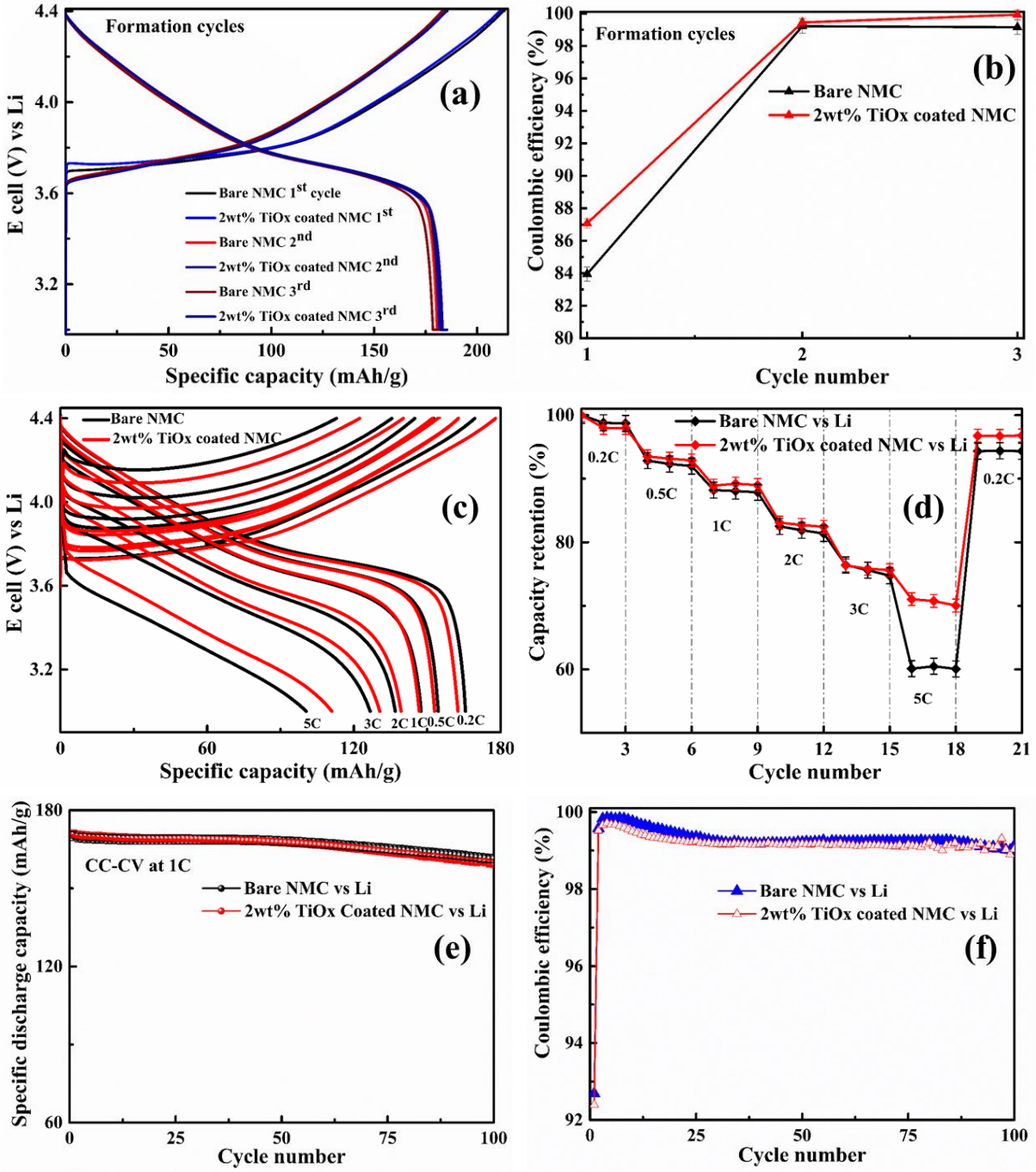


***Figure 5. Galvanostatic charge-discharge profiles (a) and the Coulombic efficiency vs cycle number of the formation cycles at C/10 (for 3 initial cycles)(b), charge-discharge profiles of NMC and $TiO_x$ coated NMC in the rate test (c) [each current step was performed for 3 cycles and the second cycle charge-discharge profile is shown], discharge capacity retention with respect to cycle number (d), life cycle test at 1C discharge rate (e) and efficiency of both NMC and coated NMC at 1C (f). [The values represent the average discharge capacity of three coin cells from the same electrode coating]***

of the discharge capacity available at 0.1C, whether this was only 60% for its NMC counterpart. This improvement in rate capability demonstrates that the thin layer of $TiO_x$ advances the kinetics of the electrochemical processes. Besides that, the cyclability of both NMC and coated NMC-622 was studied in an asymmetric charge-discharge mode (Figure 5e), i.e., all the cells were charged at 0.5C, followed by a constant voltage charging step at 4.4V (C/20 cut-off current). Subsequently, the cells were discharged at 1C. This was repeated for 100 cycles. There was no considerable difference between the cycle stability of either sample, and both showed very stable performances. The difference in Coulombic efficiency between NMC and $TiO_x$ coated NMC-622 was negligible as shown in figure 5f. The Coulombic efficiency of the first cycle was ~92.5% for both NMC and $TiO_x$ coated NMC and it was maintained above 99% for both electrodes during the investigated 100 cycles.

To better understand the effect of $TiO_x$ surface modification on NMC-622, the electrochemical impedance spectroscopy (EIS) was performed before and after cycling. The lower charge-transfer resistance for the $TiO_x$ coated samples compared to NMC both before (figure 6a) and after (figure 6b) cycling show that the $TiO_x$ coating on the NMC enhances the charge transfer kinetics. The lower charge transfer resistance ($R_{CT}$) could be related to the improved electronic percolation in the porous electrode, supported by the sheet resistance measurements, and a more stable and conductive CEI layer.

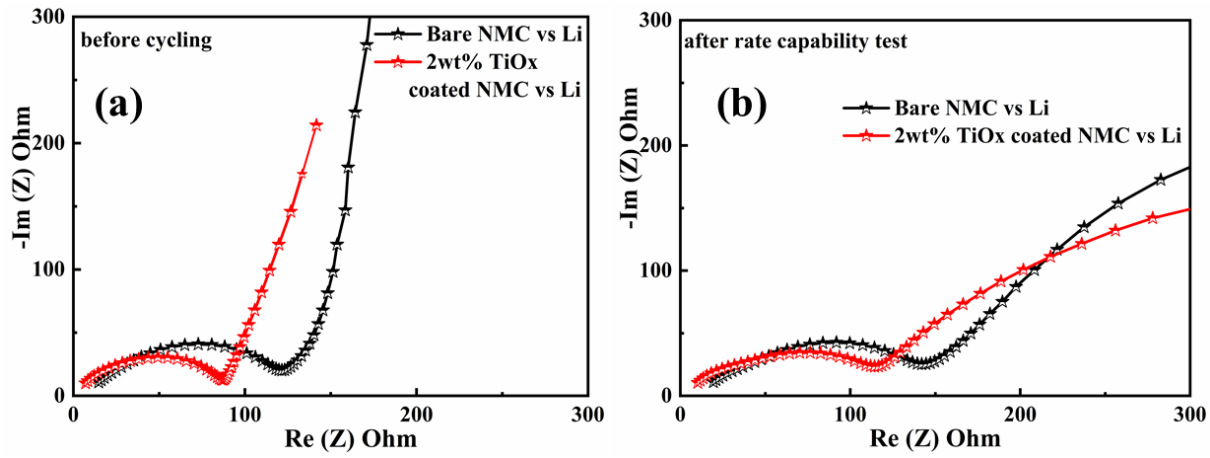


***Figure 6. EIS analysis of NMC and $TiO_x$ coated NMC before cycling (a) and after rate capability test (b).***

***NMC-LTO system:***

In commercial lithium-ion cells, graphite is commonly used as negative electrode because of its low working potential at 0.15 V vs $Li^+/Li$, enabling a high cell voltage and energy. However, the low reduction stability of conventional liquid electrolytes at the graphite electrode leads to the continuous formation of a solid electrolyte interface (SEI), to loss of cyclable lithium, and to resistance increase of the cell. Therefore, to minimize the contribution of the negative electrode in the overall aging behavior of the cell over long-term cycling, $Li_4Ti_5O_{12}$ (LTO) was used in our full cells[65]. LTO is known to have a faster kinetics, low aging rate, and zero strain [66] during prolonged cycling. LTO's high electrochemical stability can be traced back to its negligible volume expansion/reduction during lithium-ions insertion/deinsertion[66]. Its superior electrochemical stability and operating potential of 1.55 V vs $Li^+/Li$ imply that any observed capacity decay or electrochemical instability of NMC-622/LTO full cells can be directly related to the electrochemical properties of the positive electrode[67]. LTO compared to graphite has a higher stability against SEI formation, given that its redox potential is well above the reduction potential of most common conventional liquid electrolytes[68].

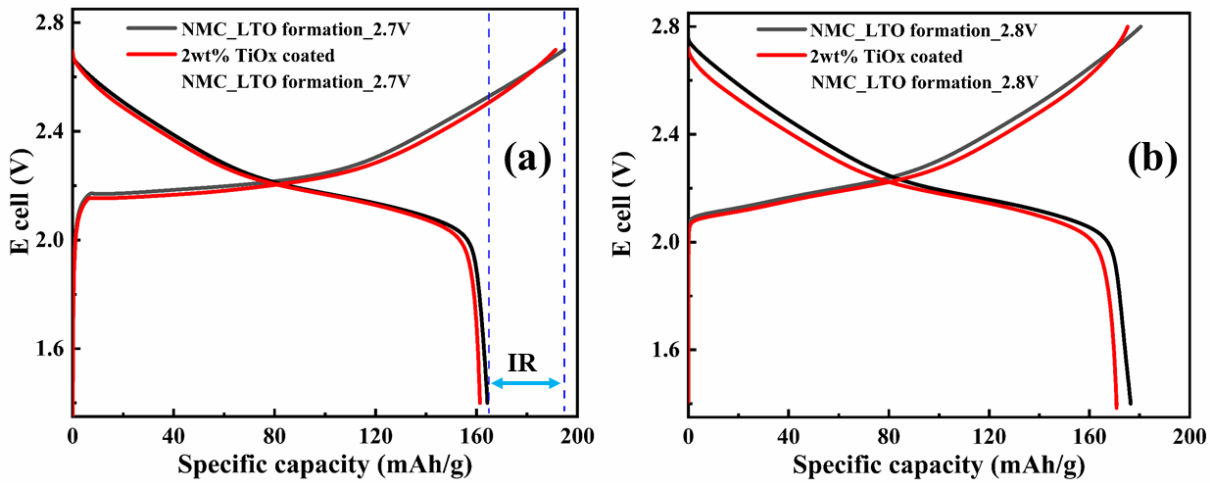


***Figure 7. Galvanostatic (formation at C/10) charge-discharge profiles of NMC-622/LTO cells, cycled between 1.4 V – 2.7 V (a) and cycled between 1.4 V – 2.8 V.***

Figure 7 shows the electrochemical characterization of ($TiO_x$ coated) NMC-622/LTO full cells, cycled between 1.4 V and 2.7 V in the formation cycles (at a current rate of C/10), and between 1.4 V - 2.8 V in the second formation cycle. Figure 7a shows the charge-discharge profiles of both NMC and 2 wt.% $TiO_x$ coated NMC/LTO full cells charged until 2.7V. However, both samples delivered the initial charge capacity of 195 ±2 mAh/g. Although the initial discharge capacity was ~162 mAh/g, it causes more than 16% of irreversible capacity loss during the initial formation cycle, related to the electrolyte decomposition and CEI growth. Besides that, the irreversible capacity loss was negligible in the second formation cycle charged until 2.8V (figure 7b), which is because of the stable CEI formation, which further helps in the long-term cycling stability.

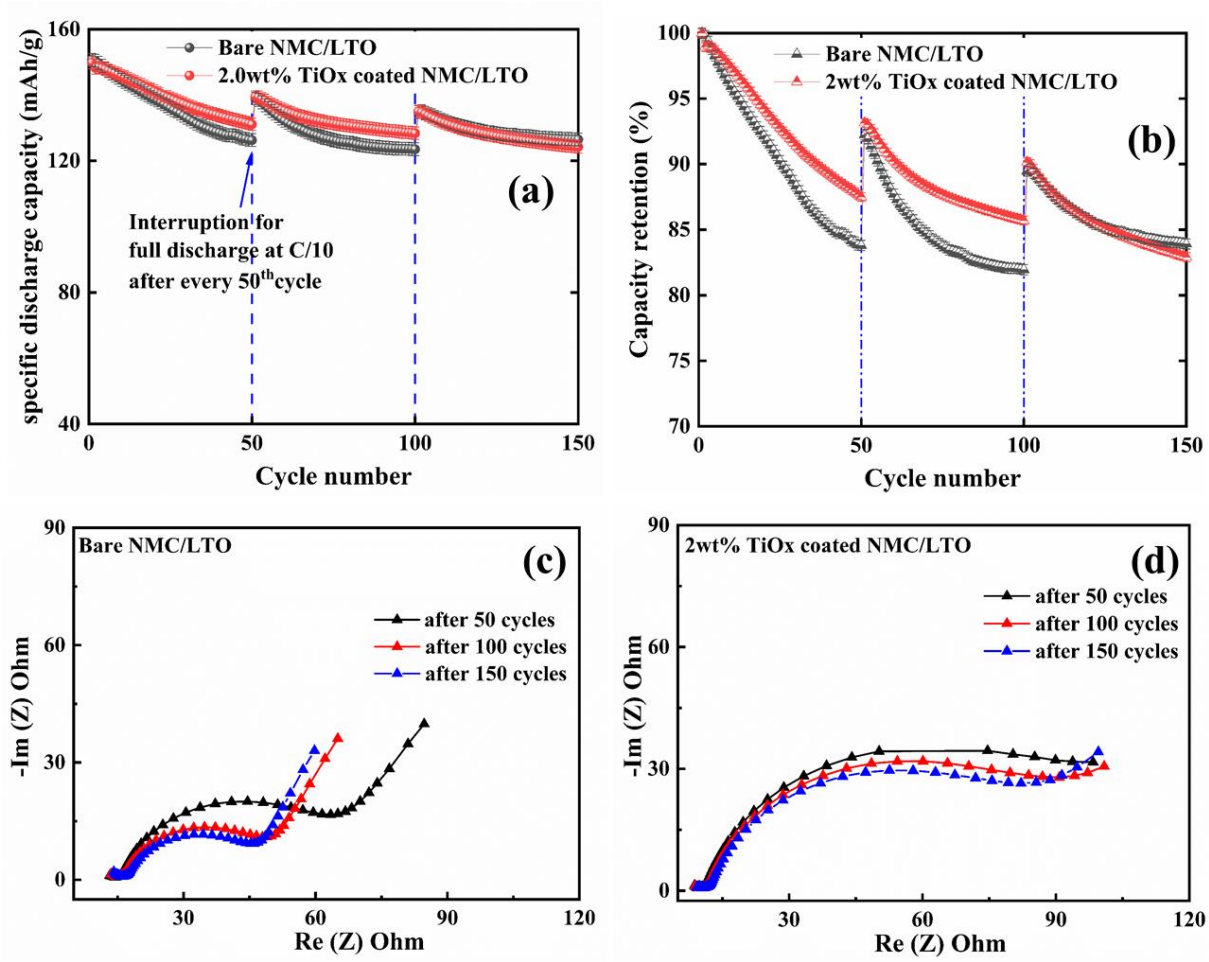


***Figure 8. Electrochemical properties of $TiO_x$ coated and NMC-622/LTO cells, discharge capacity (mAh/g) vs cycle number (a), Capacity retention (%) vs cycle number (b), Nyquist plots of NMC-LTO cells over cycling (c) and Nyquist plots of $TiO_x$ coated NMC-622/LTO cells over studied 150 cycles (d).***

The capacity retention was investigated at 1C (constant current/CC mode for 150 cycles). An intermittent characterization step was used after every 50 cycles to perform the EIS (rested at OCV for 1h before EIS) and full charge (discharge) for one cycle at C/10 (Figure 8a). In the initial cycles, NMC-622/LTO cells delivered a slightly higher average discharge capacity (avg. ca. 150.72 ± 3mAh/g) than the $TiO_x$ coated NMC-622/LTO cells (avg. ca. 149.83 ± 2mAh/g). The capacity fade of the 2 wt.% $TiO_x$ coated NMC-622/LTO was lower than NMC-622/LTO cells in the initial 50cycles. In the initial 100 cycles, the $TiO_x$ coated NMC-622 experienced a considerably lower capacity decline than its bare counterpart. Figure 8b shows the discharge capacity retention (%) vs. cycle number over the investigated 150 cycles. In the initial 50 cycles, the $TiO_x$ coated NMC-622/LTO cells exhibited higher capacity retention (~88%) than NMC-622/LTO cells (~83.7%). In the subsequent 50 to 100 cycles, $TiO_x$ coated NMC-622/LTO cells retained their capacity retention at 88%, whereas NMC-622/LTO cells further dropped to 81.9%. The enhanced capacity retention would be related to the protective behavior of $TiO_x$ coating on the NMC particles. The discharge profiles of (coated)NMC/LTO cells at initial cycle and last cycle just before the interruption have been shown in the figure S8.

Figures 8c and 8d show the EIS Nyquist plots for the NMC and $TiO_x$ coated NMC-622/LTO cells respectively. The EIS was performed during intermittent characterization periods and after a discharge at C/10 to fully lithiated state. For the uncoated NMC electrode, the charge transfer resistance decreased between $50^{th}$ to $100^{th}$ cycles and stabilized thereafter. The EIS spectra for $TiO_x$ coated samples, however stabilized only after 50 cycles, which can be interpreted as a higher stability of the cathode interface layer for the NMC particles and is in line with the lower average rate of capacity loss for the coated samples. For instance, the % loss of capacity between cycles 50 and 100 is ~7% higher for the uncoated relative to the coated samples (figure 8b). Please be advised that although our results suggest a more facilitated exchange of lithium at the electrode/electrolyte interface for the $TiO_x$-coated NMC, the

underlying mechanisms are not limited to the improved electronic conductivity and CEI properties. One needs to consider other possible contributions, to be investigated by further research, such as pseudo-capacitance reported for the similar systems[69,70].

In summary, the $TiO_x$ surface coating effectively improves the electronic conductivity of the NMC samples and provides sufficient electronic percolation at the electrode level. It is crucial to investigate the effect of coating layer thickness and the weight % of the coating materials, as they could significantly influence the electrochemical properties of the electrode materials. In this article, 10 wt.% $TiO_x$ surface modification showed higher electronic conductivity than the rest of the samples. However, it suffers from the faster Li-ion kinetics due to the shell thickness. Besides that, the desired thickness and sufficient electronic conductivity could be achieved by lowering the weight % of the coating material. Furthermore, the rate-capability (Li-ion kinetics at higher current rates), capacity retention, and interfacial stability of the NMC electrode have been enhanced by the 2 wt.% $TiO_x$ coating on NMC materials.

**Conclusions:**

In this work, a continuous thin $TiO_x$ layer was deposited on NMC-622 particles by a simple wet chemical hydrolysis deposition method. The role of aqueous ammonia during the coating process was investigated, and it was concluded that its concentration was critical to control the shell deposition. The surface modification process did not adversely affect the bulk crystalline properties and morphologies of the core particles. Furthermore, the $TiO_x$ coating improved the rate capability of NMC-622 in half-cell configuration. The electrochemical stability of NMC-622/LTO full cells was considerably improved at 1C when $TiO_x$ coated NMC-622 was used as positive electrode. These effects may be ascribed to the coating acting as a protecting layer. This work clearly shows that the material level improvements are the key parameter to improve the power density and cyclability of Ni-rich NMC based cathode materials at the full cell level.

**Acknowledgements:**

The authors acknowledge the Research Foundation Flanders (FWO, Vlaanderen) SBO XL-Lion project for the financial support (number S001017). S.K.M. would like to acknowledge the UHasselt for the PhD scholarship. The authors also thank Dr. Ken Elen for the XRD measurements, Hilde Pellaers for the SEM sample preparation, Ulrique Vounckx, Maria Batuk and Joke Haderman for the TEM analysis and Hamid Hamed for the fruitful discussions concerning the electrode preparation.

**Conflict of interest:**

The authors express no conflict of interest.

**Details of the supporting information:** The supporting information consists of the surface morphologies of the $TiO_x$ coated NMC samples, electronic conductivity measurements of both electrode level and powder samples. Also, included the XRD patterns, SEM and HR-TEM analysis of $TiO_x$ coated NMC samples. Discussion about the electrochemical impedance analysis and NMC-LTO full cells both capacity retention and discharge profiles were included as well.

**Graphical abstract:**

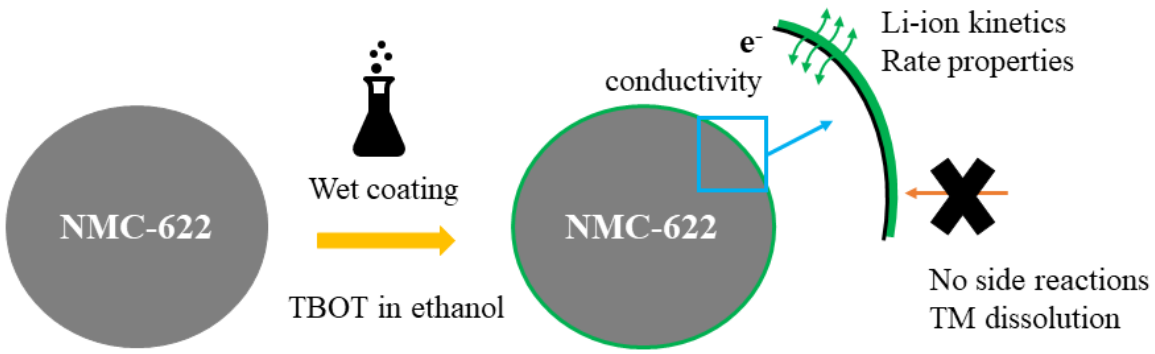

**References:**


(1) Sun, Y. K.; Myung, S. T.; Park, B. C.; Prakash, J.; Belharouak, I.; Amine, K. High-Energy Cathode Material for Long-Life and Safe Lithium Batteries. *Nat. Mater.* **2009**, *8* (4), 320–324. https://doi.org/10.1038/nmat2418.

(2) Schmuch, R.; Wagner, R.; Hörpel, G.; Placke, T.; Winter, M. Performance and Cost of Materials for Lithium-Based Rechargeable Automotive Batteries. *Nat. Energy* **2018**, *3* (4), 267–278. https://doi.org/10.1038/s41560-018-0107-2.

(3) Manthiram, A.; Song, B.; Li, W. A Perspective on Nickel-Rich Layered Oxide Cathodes for Lithium-Ion Batteries. *Energy Storage Mater.* **2017**, *6* (October 2016), 125–139. https://doi.org/10.1016/j.ensm.2016.10.007.

(4) Xu, J.; Lin, F.; Doeff, M. M.; Tong, W. A Review of Ni-Based Layered Oxides for Rechargeable Li-Ion Batteries. *J. Mater. Chem. A* **2017**, *5* (3), 874–901. https://doi.org/10.1039/C6TA07991A.

(5) Li, W.; Erickson, E. M.; Manthiram, A. High-Nickel Layered Oxide Cathodes for Lithium-Based Automotive Batteries. *Nat. Energy* **2020**, *5* (1), 26–34. https://doi.org/10.1038/s41560-019-0513-0.

(6) Manthiram, A. A Reflection on Lithium-Ion Battery Cathode Chemistry. *Nat. Commun.* **2020**, *11* (1), 1–9. https://doi.org/10.1038/s41467-020-15355-0.

(7) Ryu, H. H.; Park, K. J.; Yoon, C. S.; Sun, Y. K. Capacity Fading of Ni-Rich Li[NixCoyMn1-x-y]O2 ($0.6 \leq x \leq 0.95$) Cathodes for High-Energy-Density Lithium-Ion Batteries: Bulk or Surface Degradation? *Chem. Mater.* **2018**, *30* (3), 1155–1163. https://doi.org/10.1021/acs.chemmater.7b05269.

(8) Kim, J. H.; Ryu, H. H.; Kim, S. J.; Yoon, C. S.; Sun, Y. K. Degradation Mechanism of Highly Ni-Rich Li[NixCoyMn1- x- y]O2 Cathodes with $x > 0.9$. *ACS Appl. Mater. Interfaces* **2019**, *11* (34), 30936–30942. https://doi.org/10.1021/acsami.9b09754.

(9) Schweidler, S.; De Biasi, L.; Hartmann, P.; Brezesinski, T.; Janek, J. Kinetic Limitations in Cycled Nickel-Rich NCM Cathodes and Their Effect on the Phase Transformation Behavior. *ACS Appl. Energy Mater.* **2020**, *3* (3), 2821–2827. https://doi.org/10.1021/acsaem.9b02483.

(10) Ruan, Y.; Song, X.; Fu, Y.; Song, C.; Battaglia, V. Structural Evolution and Capacity Degradation Mechanism of LiNi0.6Mn0.2Co0.2O2 Cathode Materials. *J. Power Sources* **2018**, *400* (May), 539–548. https://doi.org/10.1016/j.jpowsour.2018.08.056.

(11) Quilty, C. D.; Bock, D. C.; Yan, S.; Takeuchi, K. J.; Takeuchi, E. S.; Marschilok, A. C. Probing Sources of Capacity Fade in LiNi0.6Mn0.2Co0.2O2 (NMC622): An Operando XRD Study of Li/NMC622 Batteries during Extended Cycling. *J. Phys. Chem. C* **2020**, *124* (15), 8119–8128. https://doi.org/10.1021/acs.jpcc.0c00262.

(12) Young-Min Choi, S.-I. P. and S.-I. M. Effects of Cation Mixing on the Electrochemical Lithium Intercalation Reaction into Porous Li 1-XNi1-YCoyO2 Electrodes. *Solid State Ionics* **1996**, *89*, 43–52.

(13) Reale, P.; Privitera, D.; Panero, S.; Scrosati, B. An Investigation on the Effect of Li+/Ni2+ Cation Mixing on Electrochemical Performances and Analysis of the Electron Conductivity Properties of LiCo0.33Mn0.33Ni0.33O2. *Solid State Ionics* **2007**, *178* (23–24), 1390–1397. https://doi.org/10.1016/j.ssi.2007.07.016.

(14) Liu, W.; Oh, P.; Liu, X.; Lee, M. J.; Cho, W.; Chae, S.; Kim, Y.; Cho, J. Nickel-Rich Layered Lithium Transition-Metal Oxide for High-Energy Lithium-Ion Batteries. *Angew. Chemie - Int. Ed.* **2015**, *54* (15), 4440–4457. https://doi.org/10.1002/anie.201409262.

(15) Li, H.; Liu, A.; Zhang, N.; Wang, Y.; Yin, S.; Wu, H.; Dahn, J. R. An Unavoidable Challenge for Ni-Rich Positive Electrode Materials for Lithium-Ion Batteries. *Chem. Mater.* **2019**, *31* (18), 7574–7583. https://doi.org/10.1021/acs.chemmater.9b02372.

(16) Chen, Z.; Qin, Y.; Amine, K.; Sun, Y. K. Role of Surface Coating on Cathode Materials for Lithium-Ion Batteries. *J. Mater. Chem.* **2010**, *20* (36), 7606–7612. https://doi.org/10.1039/c0jm00154f.

(17) Weber, D.; Tripković, Đ.; Kretschmer, K.; Bianchini, M.; Brezesinski, T. Surface Modification Strategies for Improving the Cycling Performance of Ni-Rich Cathode Materials. *Eur. J. Inorg. Chem.* **2020**, *2020* (33), 3117–3130. https://doi.org/10.1002/ejic.202000408.

(18) Han, B.; Key, B.; Lapidus, S. H.; Garcia, J. C.; Iddir, H.; Vaughey, J. T.; Dogan, F. From Coating to Dopant: How the Transition Metal Composition Affects Alumina Coatings on Ni-Rich Cathodes. *ACS Appl. Mater. Interfaces* **2017**, *9* (47), 41291–41302. https://doi.org/10.1021/acsami.7b13597.

(19) Xu, C.; Märker, K.; Lee, J.; Mahadevegowda, A.; Reeves, P. J.; Day, S. J.; Groh, M. F.; Emge, S. P.; Ducati, C.; Layla Mehdi, B.; Tang, C. C.; Grey, C. P. Bulk Fatigue Induced by Surface Reconstruction in Layered Ni-Rich Cathodes for Li-Ion Batteries. *Nat. Mater.* **2021**, *20* (1), 84–92. https://doi.org/10.1038/s41563-020-0767-8.

(20) Chen, Z.; Chao, D.; Lin, J.; Shen, Z. Recent Progress in Surface Coating of Layered LiNixCoyMnzO2 for Lithium-Ion Batteries. *Mater. Res. Bull.* **2017**, *96*, 491–502. https://doi.org/10.1016/j.materresbull.2017.05.021.

(21) Li, C.; Zhang, H. P.; Fu, L. J.; Liu, H.; Wu, Y. P.; Rahm, E.; Holze, R.; Wu, H. Q. Cathode Materials Modified by Surface Coating for Lithium Ion Batteries. *Electrochim. Acta* **2006**, *51* (19), 3872–3883. https://doi.org/10.1016/j.electacta.2005.11.015.

(22) Weigel, T.; Schipper, F.; Erickson, E. M.; Susai, F. A.; Markovsky, B.; Aurbach, D. Structural and Electrochemical Aspects of LiNi 0.8 Co 0.1 Mn 0.1 O 2 Cathode Materials Doped by Various Cations. *ACS Energy Lett.* **2019**, *4* (2), 508–516.

https://doi.org/10.1021/acsenergylett.8b02302.

(23) Zhao, Y.; Li, J.; Dahn, J. R. Interdiffusion of Cations from Metal Oxide Surface Coatings into LiCoO2 during Sintering. *Chem. Mater.* **2017**, *29* (12), 5239–5248. https://doi.org/10.1021/acs.chemmater.7b01219.

(24) Meng, X.; Yang, X.; Sun, X. Emerging Applications of Atomic Layer Deposition for Lithium-Ion Battery Studies. *Adv. Mater.* **2012**, *24*, 3589–3615. https://doi.org/10.1002/adma.201200397.

(25) Guan, C.; Wang, J. Recent Development of Advanced Electrode Materials by Atomic Layer Deposition for Electrochemical Energy Storage. *Adv. Sci.* **2016**, *3* (10), 1–23. https://doi.org/10.1002/advs.201500405.

(26) Wise, A. M.; Ban, C.; Weker, J. N.; Misra, S.; Cavanagh, A. S.; Wu, Z.; Li, Z.; Whittingham, M. S.; Xu, K.; George, S. M.; Toney, M. F. Effect of Al2O3 Coating on Stabilizing LiNi0.4Mn0.4Co0.2O2 Cathodes. *Chem. Mater.* **2015**, *27* (17), 6146–6154. https://doi.org/10.1021/acs.chemmater.5b02952.

(27) Negi, R. S.; Culver, S. P.; Mazilkin, A.; Brezesinski, T.; Elm, M. T. Enhancing the Electrochemical Performance of LiNi0.70Co0.15Mn0.15O2Cathodes Using a Practical Solution-Based Al2O3Coating. *ACS Appl. Mater. Interfaces* **2020**, *12* (28), 31392–31400. https://doi.org/10.1021/acsami.0c06484.

(28) Laskar, M. R.; Jackson, D. H. K.; Xu, S.; Hamers, R. J.; Morgan, D.; Kuech, T. F. Atomic Layer Deposited MgO: A Lower Overpotential Coating for Li[Ni0.5Mn0.3Co0.2]O2 Cathode. *ACS Appl. Mater. Interfaces* **2017**, *9* (12), 11231–11239. https://doi.org/10.1021/acsami.6b16562.

(29) Zhang, X.; Belharouak, I.; Li, L.; Lei, Y.; Elam, J. W.; Nie, A.; Chen, X.; Yassar, R. S.; Axelbaum, R. L. Structural and Electrochemical Study of Al2O3 and TiO2 Coated Li1.2Ni0.13Mn0.54Co 0.13O2 Cathode Material Using ALD. *Adv. Energy Mater.*

**2013**, *3* (10), 1299–1307. https://doi.org/10.1002/aenm.201300269.

(30) Qin, C.; Cao, J.; Chen, J.; Dai, G.; Wu, T.; Chen, Y.; Tang, Y.; Li, A.; Chen, Y. Improvement of Electrochemical Performance of Nickel Rich LiNi0.6Co0.2Mn0.2O2 Cathode Active Material by Ultrathin TiO2 Coating. *Dalt. Trans.* **2016**, *45* (23), 9669–9675. https://doi.org/10.1039/c6dt01764a.

(31) Sun, Y.-K.; Cho, S.-W.; Lee, S.-W.; Yoon, C. S.; Amine, K. AlF3-Coating to Improve High Voltage Cycling Performance of Li[Ni1⁄3Co1⁄3Mn1⁄3]O2 Cathode Materials for Lithium Secondary Batteries. *J. Electrochem. Soc.* **2007**, *154* (3), A168. https://doi.org/10.1149/1.2422890.

(32) Henderick, L.; Hamed, H.; Mattelaer, F.; Minjauw, M.; Meersschaut, J.; Dendooven, J.; Safari, M.; Vereecken, P.; Detavernier, C. Atomic Layer Deposition of Nitrogen-Doped Al Phosphate Coatings for Li-Ion Battery Applications. *ACS Appl. Mater. Interfaces* **2020**, *12* (23), 25949–25960. https://doi.org/10.1021/acsami.0c05585.

(33) Liu, W.; Li, X.; Xiong, D.; Hao, Y.; Li, J.; Kou, H.; Yan, B.; Li, D.; Lu, S.; Koo, A.; Adair, K.; Sun, X. Significantly Improving Cycling Performance of Cathodes in Lithium Ion Batteries: The Effect of Al2O3 and LiAlO2 Coatings on LiNi0.6Co0.2Mn0.2O2. *Nano Energy* **2018**, *44* (October 2017), 111–120. https://doi.org/10.1016/j.nanoen.2017.11.010.

(34) Kim, H.; Kim, M. G.; Jeong, H. Y.; Nam, H.; Cho, J. A New Coating Method for Alleviating Surface Degradation of LiNi0.6Co0.2Mn0.2O2 Cathode Material: Nanoscale Surface Treatment of Primary Particles. *Nano Lett.* **2015**, *15* (3), 2111–2119. https://doi.org/10.1021/acs.nanolett.5b00045.

(35) Zhang, W.; Chi, Z. X.; Mao, W. X.; Lv, R. W.; Cao, A. M.; Wan, L. J. One-Nanometer-Precision Control of Al2O3 Nanoshells through a Solution-Based Synthesis Route. *Angew. Chemie - Int. Ed.* **2014**, *53* (47), 12776–12780.

https://doi.org/10.1002/anie.201406856.

(36) Zhang, C.; Liu, X.; Su, Q.; Wu, J.; Huang, T.; Yu, A. Enhancing Electrochemical Performance of LiMn2O4 Cathode Material at Elevated Temperature by Uniform Nanosized TiO2 Coating. *ACS Sustain. Chem. Eng.* **2017**, *5*, 640–647. https://doi.org/10.1021/acssuschemeng.6b02011.

(37) Chen, Z.; Wang, Z.; Kim, G.; Yang, G.; Wang, H.; Wang, X.; Huang, Y.; Passerini, S.; Shen, Z. Enhancing the Electrochemical Performance of LiNi0.4Co0.2Mn0.4O2 by V2O5/LiV3O8 Coating. *ACS Appl. Mater. Interfaces* **2019**, *11*, 26994–27003. https://doi.org/10.1021/acsami.9b08591.

(38) Kim, S.; Kim, M.; Kwak, D.; Kim, D.; Lee, G.; Choe, H.; Park, K. Highly Stable TiO2 Coated Li2 MnO3 Cathode Materials for Lithium-Ion Batteries. *J. Power Sources* **2016**, *304*, 119–127. https://doi.org/10.1016/j.jpowsour.2015.11.020.

(39) Schwartz, R. W.; Schneller, T.; Waser, R. Chemical Solution Deposition of Electronic Oxide Films. *Comptes Rendus Chim.* **2004**, *7* (5), 433–461. https://doi.org/10.1016/j.crci.2004.01.007.

(40) Gao, H.; Zeng, X.; Hu, Y.; Tileli, V.; Li, L.; Ren, Y.; Meng, X.; Maglia, F.; Lamp, P.; Kim, S. J.; Amine, K.; Chen, Z. Modifying the Surface of a High-Voltage Lithium-Ion Cathode. *ACS Appl. Energy Mater.* **2018**, *1* (5), 2254–2260. https://doi.org/10.1021/acsaem.8b00323.

(41) Xin, F.; Zhou, H.; Chen, X.; Zuba, M.; Chernova, N.; Zhou, G.; Whittingham, M. S. Li-Nb-O Coating/Substitution Enhances the Electrochemical Performance of the LiNi0.8Mn0.1Co0.1O2 (NMC 811) Cathode. *ACS Appl. Mater. Interfaces* **2019**, *11* (38), 34889–34894. https://doi.org/10.1021/acsami.9b09696.

(42) Xin, F.; Zhou, H.; Zong, Y.; Zuba, M.; Chen, Y.; Chernova, N. A.; Bai, J.; Pei, B.; Goel, A.; Rana, J.; Wang, F.; An, K.; Piper, L. F. J.; Zhou, G.; Whittingham, M. S.

What Is the Role of Nb in Nickel-Rich Layered Oxide Cathodes for Lithium-Ion Batteries? *ACS Energy Lett.* **2021**, *6* (4), 1377–1382. https://doi.org/10.1021/acsenergylett.1c00190.

(43) Ulu Okudur, F.; D'Haen, J.; Vranken, T.; De Sloovere, D.; Verheijen, M.; Karakulina, O. M.; Abakumov, A. M.; Hadermann, J.; Van Bael, M. K.; Hardy, A. Ti Surface Doping of LiNi0.5Mn1.5O4-: δ Positive Electrodes for Lithium Ion Batteries. *RSC Adv.* **2018**, *8* (13), 7287–7300. https://doi.org/10.1039/c7ra12932g.

(44) Liu, Y.; Yang, Y. Recent Progress of TiO2 -Based Anodes for Li Ion Batteries. *J. Nanomater.* **2016**, *2016* (2). https://doi.org/doi.org/10.1155/2016/8123652.

(45) Szeifert, J. M.; Feckl, J. M.; Fattakhova-Rohlfing, D.; Liu, Y.; Kalousek, V.; Rathousky, J.; Bein, T. Ultrasmall Titania Nanocrystals and Their Direct Assembly into Mesoporous Structures Showing Fast Lithium Insertion. *J. Am. Chem. Soc.* **2010**, *132* (36), 12605–12611. https://doi.org/10.1021/ja101810e.

(46) Kessler, V. G. The Chemistry behind the Sol – Gel Synthesis of Complex Oxide Nanoparticles for Bio-Imaging Applications. *J. Sol-Gel Sci. Technol.* **2009**, *51*, 264–271. https://doi.org/10.1007/s10971-009-1946-x.

(47) Kessler, V. G.; Spijksma, G. I.; H, G. A. S. S. New Insight in the Role of Modifying Ligands in the Sol-Gel Processing of Metal Alkoxide Precursors : A Possibility to Approach New Classes of Materials. *J. Sol-Gel Sci. Technol.* **2006**, *40*, 163–179. https://doi.org/10.1007/s10971-006-9209-6.

(48) Svensson, F. G.; Seisenbaeva, G. A.; Kessler, V. G. Mixed-Ligand Titanium "Oxo Clusters": Structural Insights into the Formation and Binding of Organic Molecules and Transformation into Oxide Nanostructures on Hydrolysis and Thermolysis. *Eur. J. Inorg. Chem.* **2017**, *2017* (35), 4117–4122. https://doi.org/10.1002/ejic.201700775.

(49) Simonsen, M. E.; Søgaard, E. G. Sol-Gel Reactions of Titanium Alkoxides and Water:

Influence of PH and Alkoxy Group on Cluster Formation and Properties of the Resulting Products. *J. Sol-Gel Sci. Technol.* **2010**, *53* (3), 485–497. https://doi.org/10.1007/s10971-009-2121-0.

(50) Li, W.; Yang, J.; Wu, Z.; Wang, J.; Li, B.; Feng, S.; Deng, Y.; Zhang, F.; Zhao, D. A Versatile Kinetics-Controlled Coating Method to Construct Uniform Porous TiO 2 Shells for Multifunctional Core-Shell Structures. *J. Am. Chem. Soc.* **2012**, *134* (29), 11864–11867. https://doi.org/10.1021/ja3037146.

(51) Van Bomme, A.; Dahn, J. R. Analysis of the Growth Mechanism of Coprecipitated Spherical and Dense Nickel, Manganese, and Cobalt-Containing Hydroxides in the Presence of Aqueous Ammonia. *Chem. Mater.* **2009**, *21* (8), 1500–1503. https://doi.org/10.1021/cm803144d.

(52) Sugimoto, T.; Kojima, T. Formation Mechanism of Amorphous TiO2 Spheres in Organic Solvents. 1. Roles of Ammonia. *J. Phys. Chem. C* **2008**, *112* (48), 18760–18771. https://doi.org/10.1021/jp8029506.

(53) Wang, P.; Chen, D.; Tang, F. Q. Preparation of Titania-Coated Polystyrene Particles in Mixed Solvents by Ammonia Catalysis. *Langmuir* **2006**, *22* (10), 4832–4835. https://doi.org/10.1021/la060112p.

(54) Liu, Y.; Lin, X.; Sun, Y.; Xu, Y.; Chang, B.; Liu, C. Precise Surface Engineering of Cathode Materials for Improved Stability of Lithium-Ion Batteries. *Smal* **2019**, *1901019*, 1–17. https://doi.org/10.1002/smll.201901019.

(55) Wang, K.; Huang, S. P.; Wu, Y.; Cai, N. N.; Li, N.; Xiao, Q.; Sun, Z. Critical Thickness of a Surface-Functionalized Coating for Enhanced Lithium Storage: A Case Study of Nanoscale Polypyrrole-Coated FeS2 as a Cathode for Li-Ion Batteries. *Nanoscale* **2019**, *11* (35), 16277–16283. https://doi.org/10.1039/c9nr05523a.

(56) Yabuuchi, N.; Koyama, Y.; Nakayama, N.; Ohzuku, T. Solid-State Chemistry and

Electrochemistry of LiCo[Sub 1⁄3]Ni[Sub 1⁄3]Mn[Sub 1⁄3]O[Sub 2] for Advanced Lithium-Ion Batteries. *J. Electrochem. Soc.* **2005**, *152* (7), A1434. https://doi.org/10.1149/1.1924227.

(57) Lee, K.-S.; Myung, S.-T.; Amine, K.; Yashiro, H.; Sun, Y.-K. Structural and Electrochemical Properties of Layered LiNi 1−2xCoxMnxO2 (X=0.1–0.3) Positive Electrode Materials for Li-Ion Batteries. *J. Electrochem. Soc.* **2007**, *154* (10), A971. https://doi.org/10.1149/1.2769831.

(58) Noh, H. J.; Youn, S.; Yoon, C. S.; Sun, Y. K. Comparison of the Structural and Electrochemical Properties of Layered Li[NixCoyMnz]O2 (x = 1/3, 0.5, 0.6, 0.7, 0.8 and 0.85) Cathode Material for Lithium-Ion Batteries. *J. Power Sources* **2013**, *233*, 121–130. https://doi.org/10.1016/j.jpowsour.2013.01.063.

(59) Julien, C.; Mauger, A.; Zaghib, K.; Groult, H. Optimization of Layered Cathode Materials for Lithium-Ion Batteries. *Materials (Basel).* **2016**, *9* (7). https://doi.org/10.3390/MA9070595.

(60) Wang, D.; Belharouak, I.; Ortega, L. H.; Zhang, X.; Xu, R.; Zhou, D.; Zhou, G.; Amine, K. Synthesis of High Capacity Cathodes for Lithium-Ion Batteries by Morphology-Tailored Hydroxide Co-Precipitation. *J. Power Sources* **2015**, *274*, 451–457. https://doi.org/10.1016/j.jpowsour.2014.10.016.

(61) Leichtweiss, T.; Henning, R. A.; Koettgen, J.; Schmidt, R. M.; Holländer, B.; Martin, M.; Wuttig, M.; Janek, J. Amorphous and Highly Nonstoichiometric Titania (TiOx) Thin Films Close to Metal-like Conductivity. *J. Mater. Chem. A* **2014**, *2* (18), 6631–6640. https://doi.org/10.1039/c3ta14816e.

(62) Singh, D. P.; Birkhölzer, Y. A.; Cunha, D. M.; Dubbelink, T.; Huang, S.; Hendriks, T. A.; Lievens, C.; Huijben, M. Enhanced Cycling and Rate Capability by Epitaxially Matched Conductive Cubic TiO Coating on LiCoO2Cathode Films. *ACS Appl. Energy*

*Mater.* **2021**, *4* (5), 5024–5033. https://doi.org/10.1021/acsaem.1c00603.

(63) Hiroki Kondo, Hiroshi Sawada, Chikaaki Okuda, and T. S. Influence of the Active Material on the Electronic Conductivity of the Positive Electrode in Lithium-Ion Batteries. *J. Electrochem. Soc.* **2019**, *166*, A1285. https://doi.org/10.1149/2.0051906jes.

(64) Müller, V.; Kaiser, R.; Poller, S.; Sauerteig, D. Importance of the Constant Voltage Charging Step during Lithium-Ion Cell Formation. *J. Energy Storage* **2018**, *15*, 256–265. https://doi.org/10.1016/j.est.2017.11.020.

(65) Yari, S.; Hamed, H.; D'Haen, J.; Van Bael, M. K.; Renner, F. U.; Hardy, A.; Safari, M. Constructive versus Destructive Heterogeneity in Porous Electrodes of Lithium-Ion Batteries. *ACS Appl. Energy Mater.* **2020**, *3* (12), 11820–11829. https://doi.org/10.1021/acsaem.0c01966.

(66) Ohzuku, T.; Ueda, A.; Yamamoto, N. Zero-Strain Insertion Material of Li [ Li1 / 3Ti5 / 3 ] O 4 for Rechargeable Lithium Cells. *J. Electrochem. Soc.* **1995**, *142* (5), 1431–1435. https://doi.org/10.1149/1.2048592.

(67) Takami, N.; Inagaki, H.; Tatebayashi, Y.; Saruwatari, H.; Honda, K.; Egusa, S. High-Power and Long-Life Lithium-Ion Batteries Using Lithium Titanium Oxide Anode for Automotive and Stationary Power Applications. *J. Power Sources* **2013**, *244*, 469–475. https://doi.org/10.1016/j.jpowsour.2012.11.055.

(68) Metzger, M.; Strehle, B.; Solchenbach, S.; Gasteiger, H. A. Origin of H2 Evolution in LIBs: H2O Reduction vs. Electrolyte Oxidation. *J. Electrochem. Soc.* **2016**, *163* (5), A798–A809. https://doi.org/10.1149/2.1151605jes.

(69) Wang, J.; Polleux, J.; Lim, J.; Dunn, B. Pseudocapacitive Contributions to Electrochemical Energy Storage in TiO 2 (Anatase) Nanoparticles. *J. Phys. Chem. C* **2007**, *111* (40), 14925–14931. https://doi.org/10.1021/jp074464w.

(70) Cunha, D. M.; Hendriks, T. A.; Vasileiadis, A.; Vos, C. M.; Verhallen, T.; Singh, D. P.; Wagemaker, M.; Huijben, M. Doubling Reversible Capacities in Epitaxial Li4Ti5O12 Thin Film Anodes for Microbatteries. *ACS Appl. Energy Mater.* **2019**, *2* (5), 3410–3418. https://doi.org/10.1021/acsaem.9b00217.